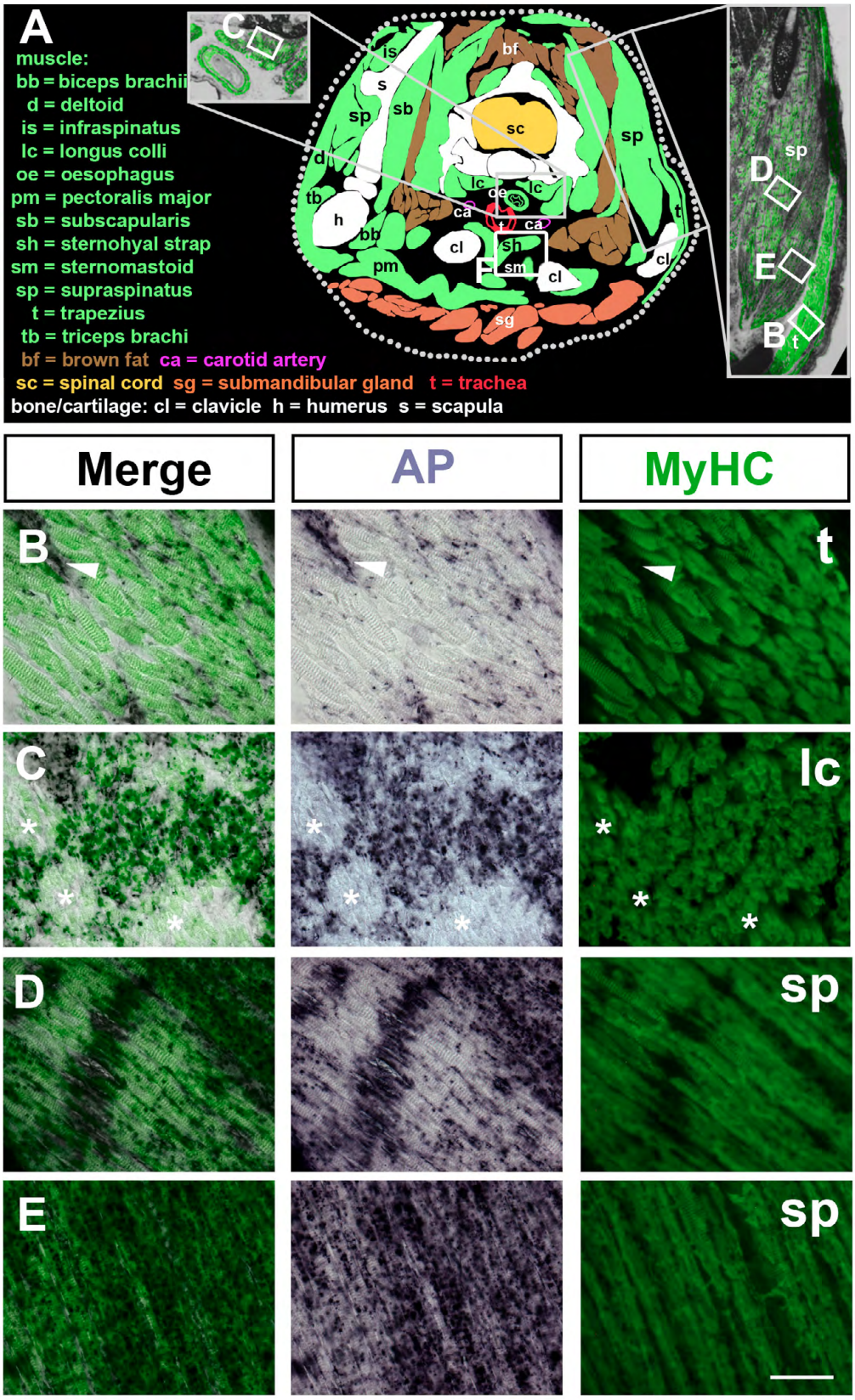

Fig. S1. Origin of cells in P0 muscle revealed by cell lineage tracing in *Pax3*^{Cre} mice. Cryosections of P0 *Pax3*^{Cre}*;Z/AP* mouse stained for alkaline phosphatase (AP, black, merge) and MyHC (green). (**A**) Schematic of a neck section at the level of the head of the right humerus where it meets the scapula (left). Insets of oesophageal (left) and left lateral (right) boxed regions, indicating anatomical location of images in B-F. (**B**) Oblique section of a cucullaris-derived trapezius muscle (t) containing little or no AP activity above that observed in sibling *Z/AP* mice lacking Cre. There is staining of Pax3-expressing putative Schwann cell precursors in intramuscular nerves (arrowhead) (Kioussi et al. 1995). (**C**) Transverse section of longus colli (lc) muscle which, although generally AP^{+}, had distinct patches of fibres lacking AP stain (asterisks). (**D**,**E**) Distinct regions of longitudinally sectioned supraspinatus muscle (sp) with marked bands (D) or more uniform staining (E). Scale bar: 50 µm in B-E.

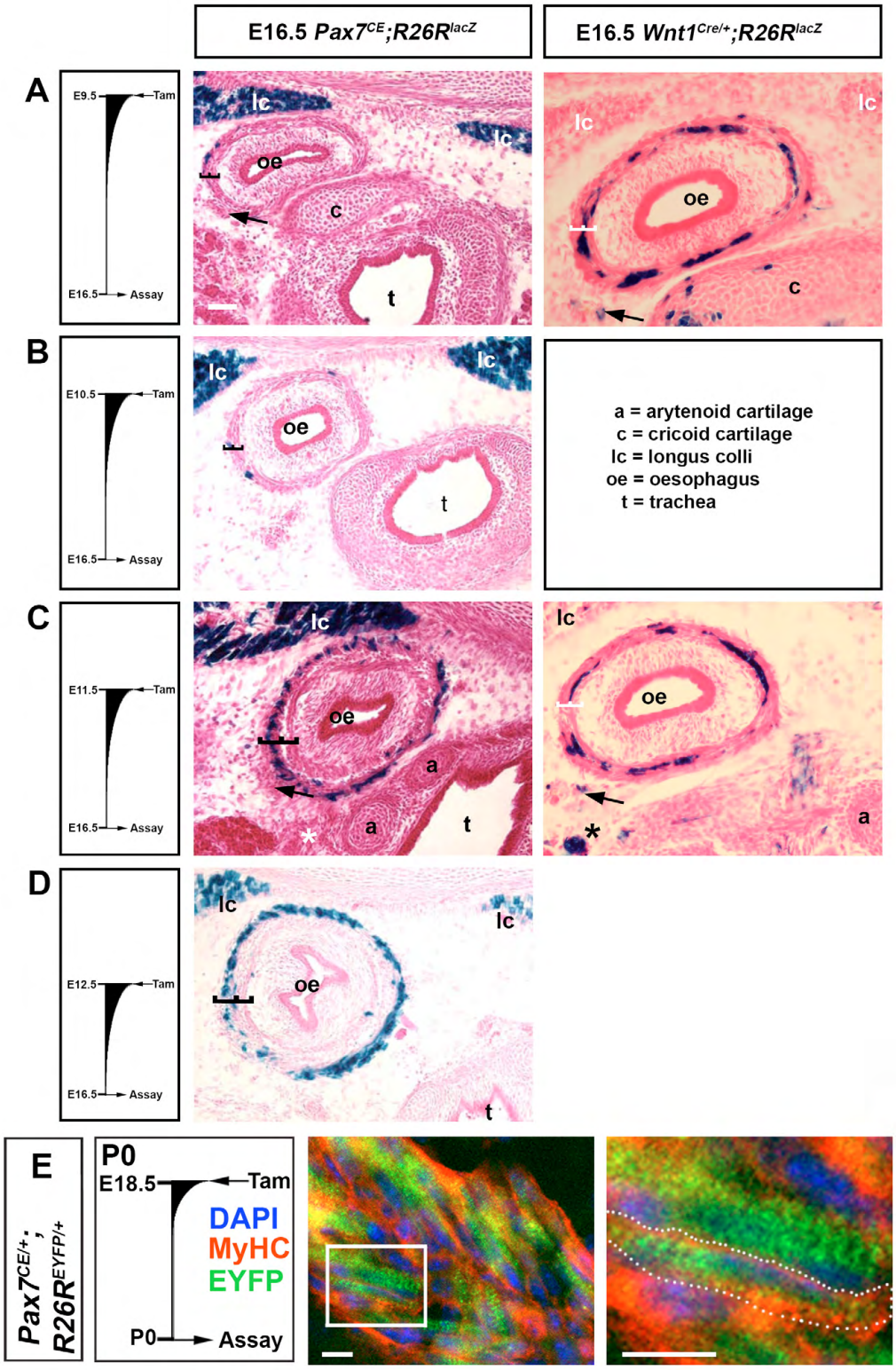

Fig. S2. Origin of cells in E16.5 oesophagus revealed by cell lineage tracing in Pax7^{CE} mice. *Wnt1^{Cre};R26R^{lacZ}* (right column) or *Pax7^{CE};R26R^{lacZ}* mice treated with tamoxifen at the indicated times (left column) were collected at E16.5 and transverse sections of the oesophagus (oe) were stained with Xgal (blue) and eosin (pink). (**A**) When tamoxifen was administered at E9.5, there were rare marked cells in outer longitudinal muscle layer at E16.5 (bracket), in which the first OSM cells have recently appeared (see Fig. 1B,D,F,I,J), and the longus capitis (lc) muscle was abundantly labelled. By contrast, *Wnt1^{Cre};R26R^{lacZ}* mice were primarily marked between the inner and outer smooth muscle layers (bracket), and in flanking nerves (arrows), which are unmarked by *Pax7^{CE};R26R^{lacZ}*. (**B**) Tamoxifen administration 1 day later, at E10.5, marked more cells at a similar cranial level, as shown by presence of tracheal (t) cartilage in the sections. (**C**) Tamoxifen treatment at E11.5 led to more abundant marking of the outer longitudinal OSM layer, but a striking lack of X-gal staining in the inner circumferential muscle layer (brackets). At the same anteroposterior level, *Wnt1^{Cre};R26R^{lacZ}* mice have marked cells between the muscle layers (brackets). (**D**) Tamoxifen administration at E12.5 marked many cells in the outer layer, and fewer cells in the inner layer (brackets). (**E**) *Pax7^{CE};R26R^{EYFP}* treated with tamoxifen at E18.5 showed EYFP marking of both inner and outer muscle layers at P0 (similar region to box H in Fig. 1J). Scale bars: 50 μm in A-D; 20 μm in E.

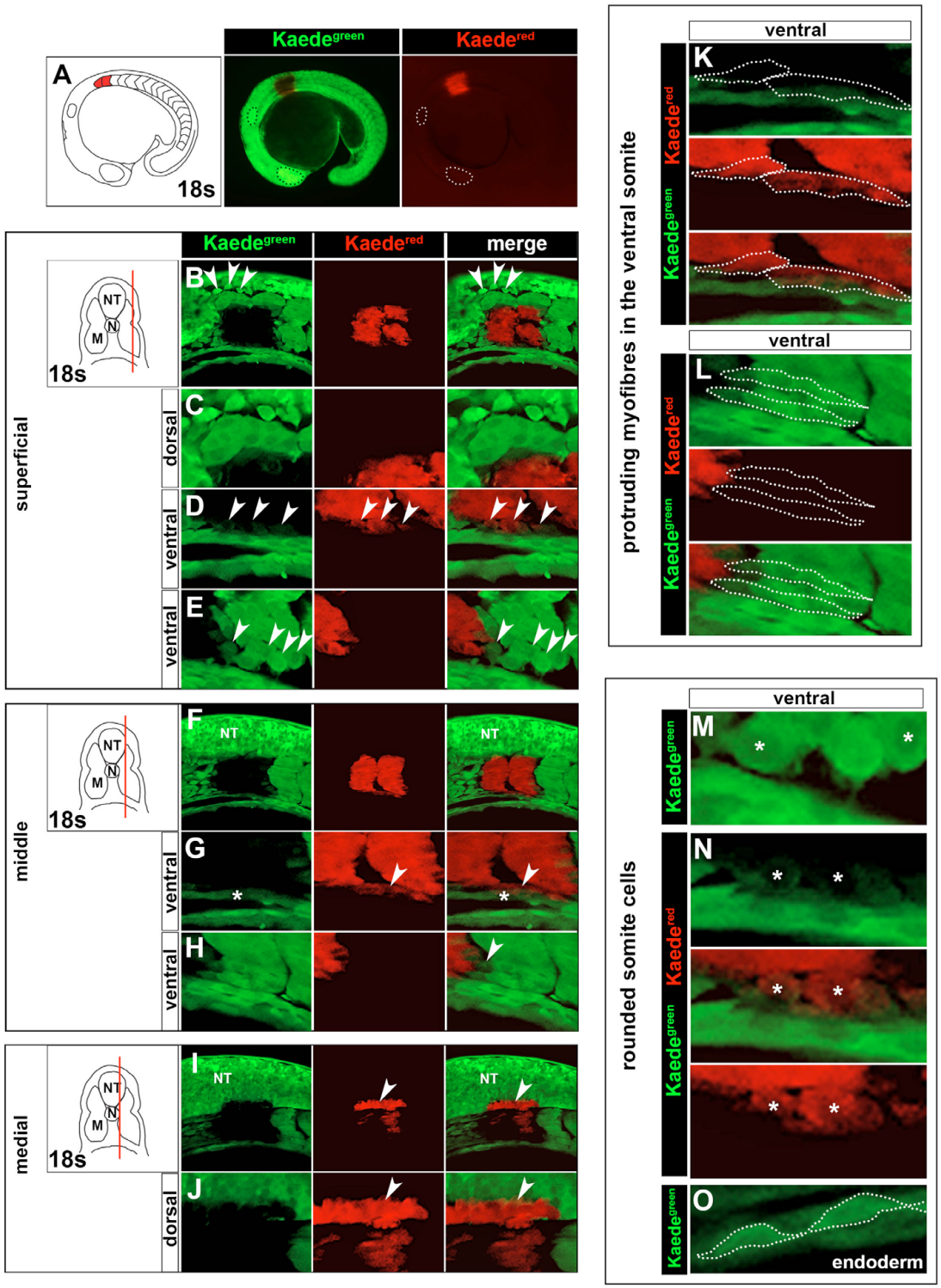

Fig. S3. Precision of Kaede photoconversion within the anterior somites of zebrafish. Primary green Kaede (Kaede^{green}) fluorescence and photoconverted red Kaede (Kaede^{red}) fluorescence. All images are whole-mount lateral views of a single embryo taken immediately after photoconversion, with anterior towards the left and dorsal towards the top. (**A**) Stereomicroscopic view of S1+2 photoconversion at 18 ss. (**B**) Superficial section through a ventral region photoconversion of S1+2 at 18 ss to avoid neural crest cells in the migratory zone (arrowheads). (**C**) Higher magnification view of unconverted neural crest cells. (**D**,**E**) Mesenchymal Kaede^{red} cells in ventral somite regions (D, arrowheads) share similar morphology to Kaede^{green} somite cells (E, arrowheads). These cells are shown at higher magnification in M,N. (**F**) Middle section through a ventral region photoconversion of S1+2 at 18 ss. (**G**,**H**) Kaede^{red} cells in ventral somite regions (G, arrowheads) are distinct from endoderm (G, asterisk) and share identical morphology to Kaede^{green} myofibres that protrude anteriorly from the ventral somite (H, arrowhead). These cells are shown at higher magnification in K,L. (**I**,**J**) Medial section through a ventral region photoconversion of S1+2 at 18 ss reveals neural tube (NT) photoconversion (arrowheads). (**K**,**L**) High magnification of Kaede^{red} or Kaede^{green} myofibres that protrude from the ventral somite (dotted lines). (**M**,**N**) Mesenchymal Kaede^{green} or Kaede^{red} ventral somite cells have similar rounded morphology distinct from fibres that includes large intracellular zones of low Kaede fluorescence (asterisks). (**O**) These ‘rounded’ somite cells are distinct from endoderm cells, which are tightly connected and have a distinctive ‘flattened’ morphology (dotted lines).

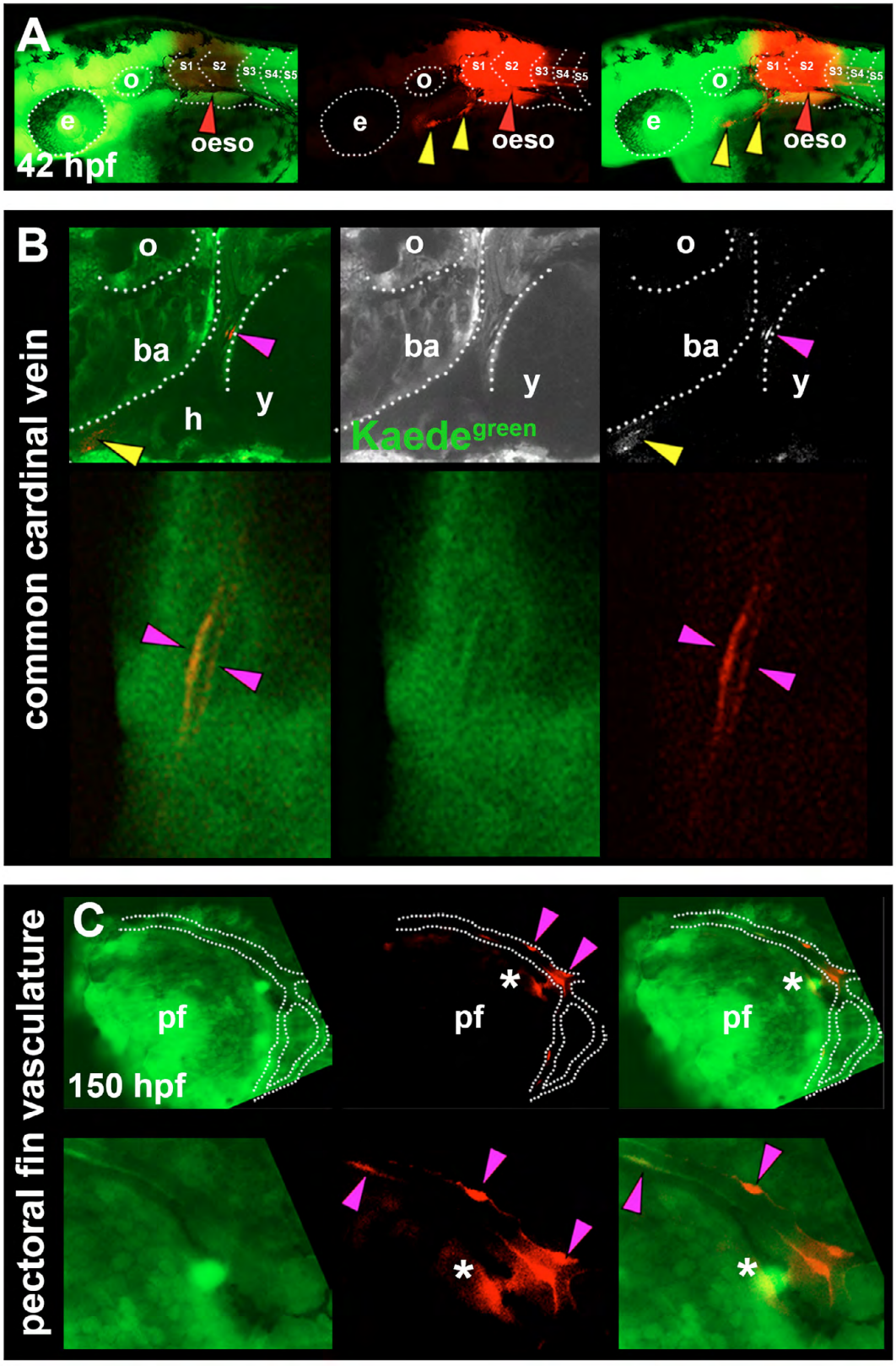

Fig. S4. Cells associated with the heart and pectoral fin vasculature are derived from anterior somites in zebrafish. Primary green Kaede (Kaede^{green}) fluorescence and photoconverted red Kaede (Kaede^{red}) fluorescence. All images are lateral view wholemounts with anterior towards the left and dorsal towards the top. (**A**) Kaede^{red} fluorescence localised to the oesophagus after photoconversion at 18 ss (red arrowheads). SHM was also labelled with Kaede^{red} (yellow arrowheads). (**B**) Photoconversion of S2 at 14-18 ss marks vascular elements associated with the common cardinal vein (magenta arrowheads) and SHM (yellow arrowheads). (**C**) In addition, cells associated with pectoral fin vasculature and other unidentified cells were labelled after photoconversion of S1/2 (magenta arrowheads and asterisks, respectively). Labelled blood vessels were observed only in tissues adjacent to the original somites converted, suggesting regional restriction of somite-derived vasculature. ba, branchial arches; oeso, oesophagus; h, heart; pf, pectoral fin; o, otic vesicle; y, yolk.

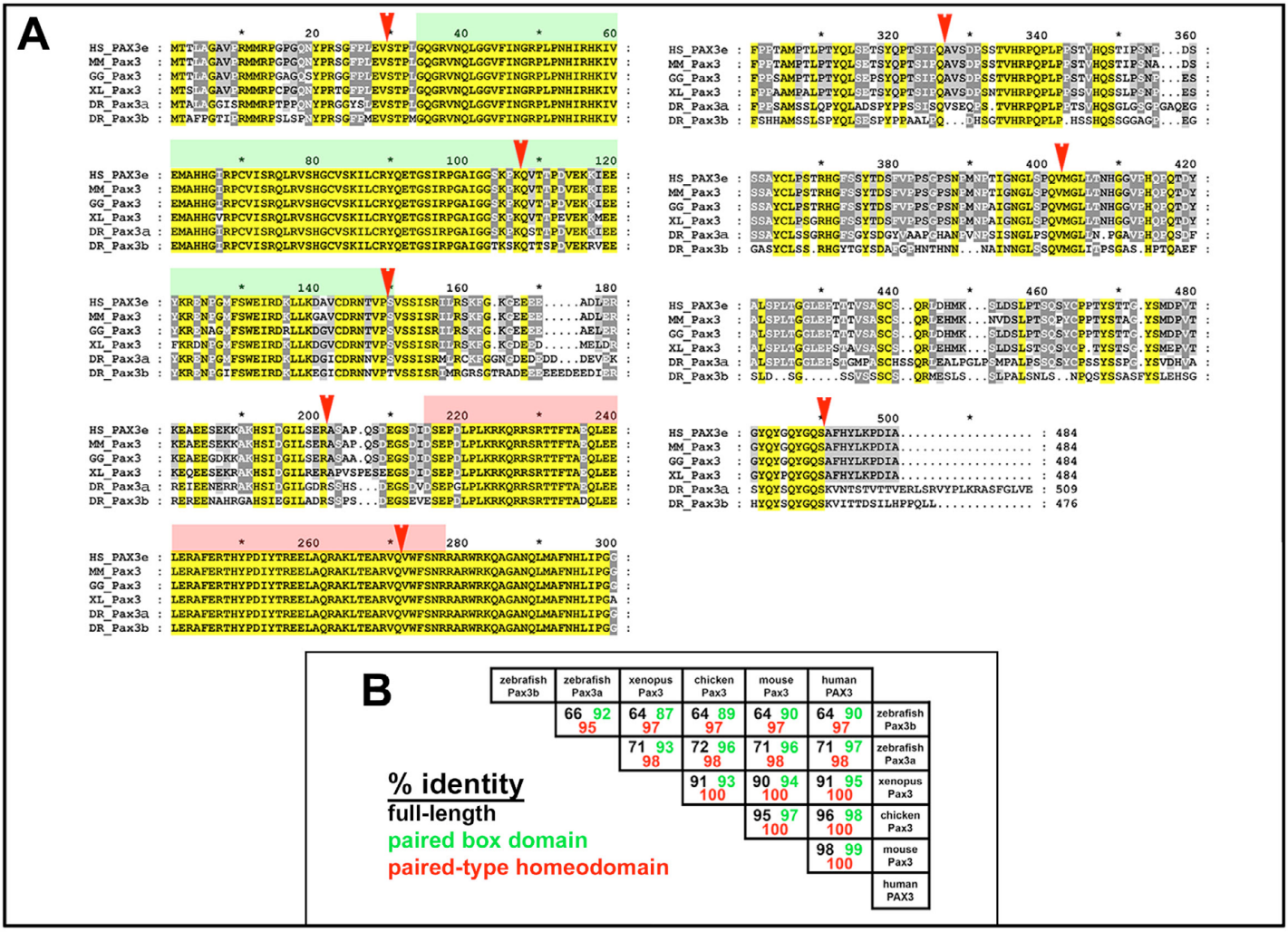

Fig. S5. Sequence comparison of zebrafish Pax3b. (**A**) Alignment of vertebrate Pax3 family proteins showing fully (yellow) and partially (grey) conserved amino acids, paired (green) and homeodomain (pink) regions, and exon borders (red arrowheads). (**B**) Pax3a has a higher level of conservation to mammalian Pax3 than does Pax3b.

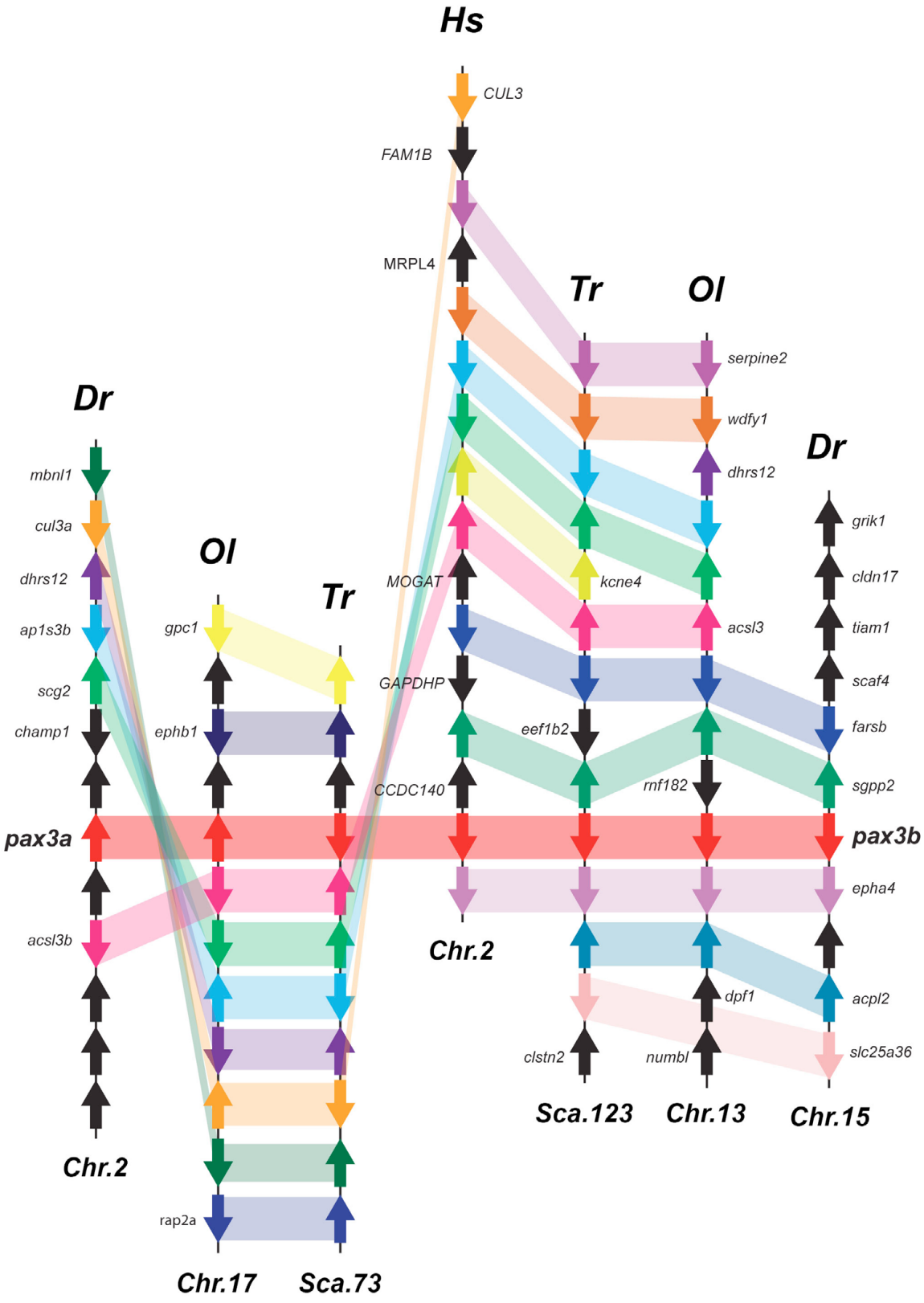

Fig. S6. Synteny analysis of Pax3 genes. ENSEMBL genomic structures (August 2012) were used to determine gene order and orientation around Pax3 loci in three species of teleost, *Danio rerio* (*Dr*, Zv9), *Takifugu rubripes* (*Tr*, FUGU4) and *Oryzias latipes* (*Ol*, MEDAKA1), and to compare with *Homo sapiens* (*Hs*, GRCh37). Gene homologues are linked by coloured ribbons to aid comparison. *pax3a* (left) and *pax3b* (right) are duplicated in teleosts, and the conserved synteny of both orthologues with *PAX3* on *Hs* chromosome 2. All three teleost *pax3b* genes retain synteny and orientation with the close neighbour human genes *FARSB* and *SGPP2* at the 5′ side and *EPH4* at the 3′ side. However, between the two major branches of teleosts, the euteleosts (*Tr* and *Ol*) retain more extensive 5′ synteny than does the ostarioclupeomorph zebrafish. Teleost *pax3a* genes also retain extensive synteny with the 5′ region of *PAX3*, but in this case zebrafish *pax3a* appears to have retained better the mammalian chromosome structure, whereas the euteleosts seem to have undergone repeated inversions.

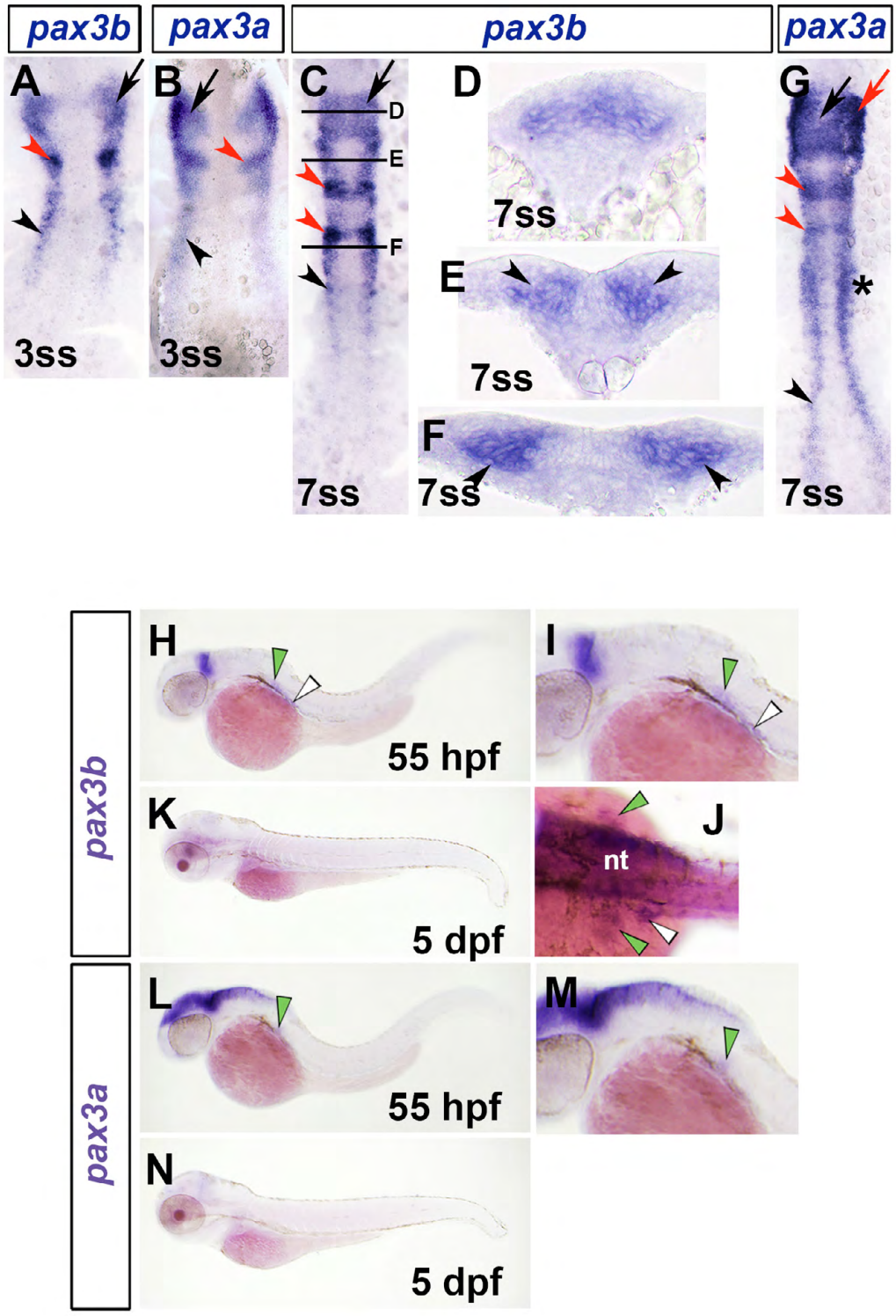

Fig. S7. Expression analysis of zebrafish *pax3a* and *pax3b*. *In situ* mRNA hybridization for *pax3b* (A,C-F,H-K) and *pax3a* (B,G,L-N). Dorsal flatmounts have anterior towards the top (A-C,G). Transverse cryosections have dorsal towards top (D-F). Lateral view wholemounts have anterior to left and dorsal to top (H,I,K-N). Dorsal wholemounts have anterior to left (J). (**A**,**B**) *pax3b* and *pax3a* mRNA at 3 ss were located in neural tissue in cranial regions (black arrow), including prospective rhombomere 2 (red arrowhead) and bilateral stripes corresponding to lateral neural plate (black arrowhead). (**C-F**) At 7 ss, *pax3b* continued to be expressed in cranial neural tissue (black arrow), including rhombomeres 2 and 4 (red arrowheads) and bilateral stripes in posterior of embryo (black arrowhead). Black bars in C denote level of section in D-F *pax3b* mRNA was located in dorsal region of neural tube within more developed neural tissue (D). Posteriorly, in less developed neural tissue (E), *pax3b* was located at lateral margin of neural plate (black arrowheads, F). (**G**) *pax3a* mRNA was also detected in lateral neural plate at 7 ss (black arrowhead), in addition to somites (asterisk), cranial neural crest (black arrow) and rhombomeres 2 and 4 (red arrowheads). (**H-K**) At subsequent embryonic (H-J, 55 hpf) but not larval (K, 5 dpf) stages, *pax3b* mRNA was detected weakly in pectoral fin (green arrowheads) and more readily in MMPs located close to the somite (white arrowheads). (**L-N**) *pax3a* mRNA was detected in pectoral fin muscle of late embryo (green arrowheads, L,M), but not larva (N). nt, neural tube.

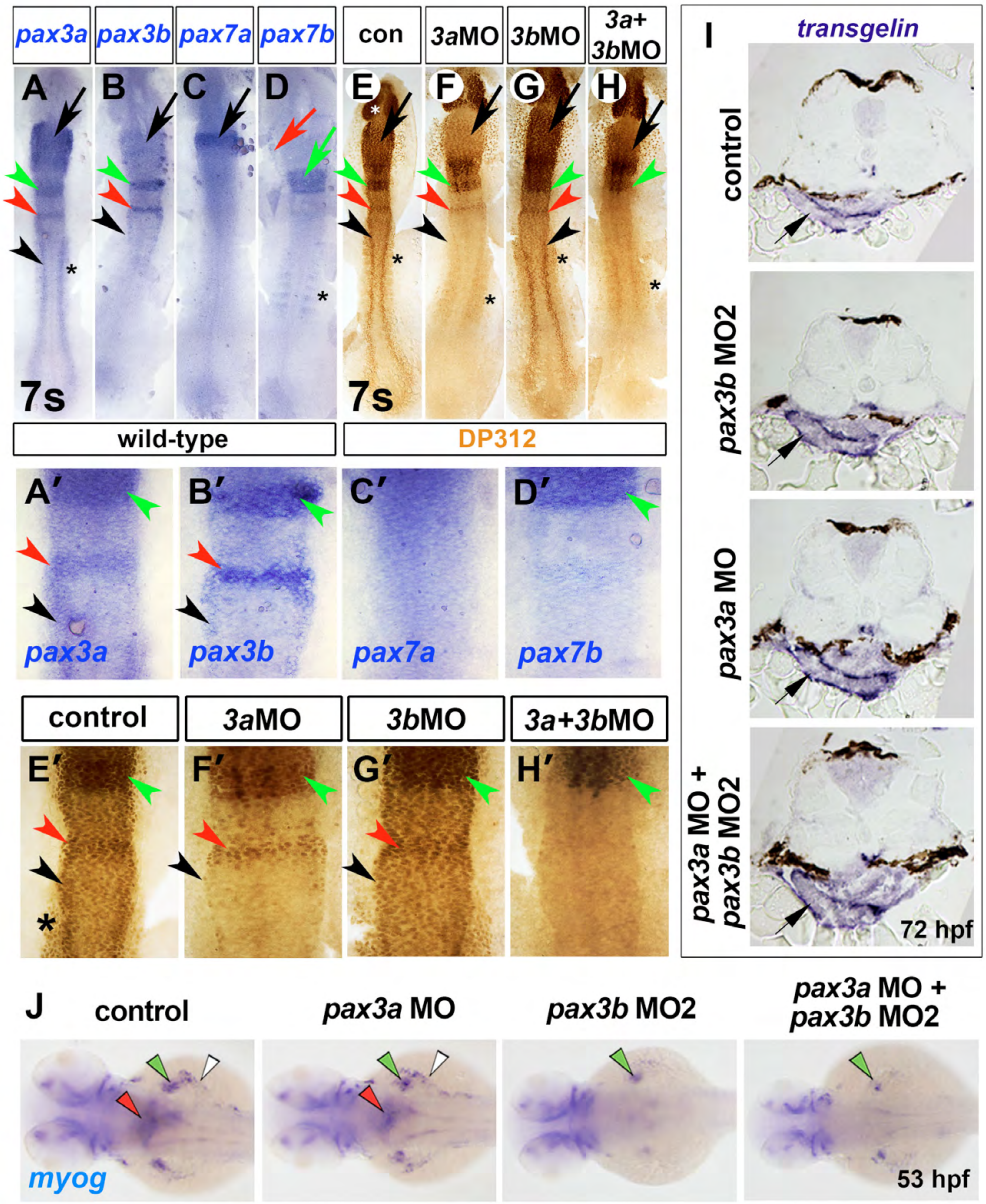

Fig. S8. *pax3b* morpholinos specifically reduce Pax3b protein but not *transgelin* expression. *In situ* mRNA hybridization for *pax3a* (A,A′), *pax3b* (B,B′), *pax7a* (C,C′), *pax7b* (D,D′), *transgelin* (I), *myog* (J) and parallel immunodetection of nuclear Pax3/7 protein (brown, DP312 antibody, E-H′) in 7 ss embryos injected with the indicated MOs. Dorsal view flatmounts with anterior towards the top (A-H′) or left (J). Transverse cryosections with dorsal towards the top (I). (**A-B′**) *pax3a* was detected in rhombomeres 2 (green arrowheads, A,A′) and 4 (red arrowheads, A,A′), lateral neural plate (black arrowheads, A,A′) and somites (asterisk, A,A′). Concurrently, *pax3b* mRNA was also observed in rhombomere 2 (green arrowhead, B,B′), rhombomere 4 (red arrowhead, B,B′) and lateral neural plate (black arrowhead, B,B′) but was lacking in somites (B,B′). (**C-D′**) The related *pax3/7* family member *pax7a* was expressed solely in the midbrain region (black arrow, C), whereas *pax7b* mRNA was detected in somites (asterisk, D) and a broad anterior hindbrain region (green arrow and arrowhead, D,D′). Therefore, of *pax3/7* family members, *pax3a* was the most widely and abundantly expressed at 7 ss, encompassing expression domains of all other *pax3/7* family members. (**E**,**E′**) Pax3/7 immunoreactivity closely resembles the sum of all *pax3/7* mRNA localisation, with the addition of signal in the forming retina owing to the known reaction of DP312 with Rx proteins (asterisks, E) (Davis et al. 2005). (**F-G′**) Injection of MO1 specific to *pax3b* did not result in a detectable reduction of Pax3/7 protein (G,G′), in agreement with residual reactivity to other Pax3/7 proteins, particularly Pax3a. After MO1-mediated Pax3a reduction (F,F′), Pax3/7 protein is clearly evident in regions of *pax3b* expression including rhombomere 2 (F,F′, green arrowheads), rhombomere 4 (F,F′, red arrowheads) and lateral neural plate (F,F′, black arrowheads), suggesting that residual Pax3/7 reactivity represents Pax3b. Using two non-overlapping *pax3a* MOs, we failed to observe the head phenotype previously described for *pax3a* knockdown (Lin et al. 2009). (**H**,**H′**) Knockdown of both Pax3b and Pax3a proteins resulted in the ablation of the residual Pax3/7 immunoreactivity in rhombomere 4 and lateral neural plate, which corresponded to Pax3b. Remaining Pax3/7 protein anteriorly is likely to reflect Pax7b protein (green arrowhead, H′) (Davis et al. 2005; Minchin and Hughes 2008). Therefore, we conclude that residual immunoreactivity after Pax3a reduction corresponds in part to Pax3b protein and that this is specifically reduced by *pax3b* MO1, which does not itself target Pax3a. Similar results were obtained with *pax3a* MO2 and *pax3b* MO2 (Table S1). (**I**) *transgelin* mRNA in oesophagus at 72 hpf did not change after *pax3* manipulation (arrows). (**J**) *myog* mRNA in oesophagus (red arrowheads), pectoral fin muscle (green arrowheads) and posterior hypaxial muscles (white arrowheads) is reduced in *pax3b* and *pax3a+pax3b* double morphants.

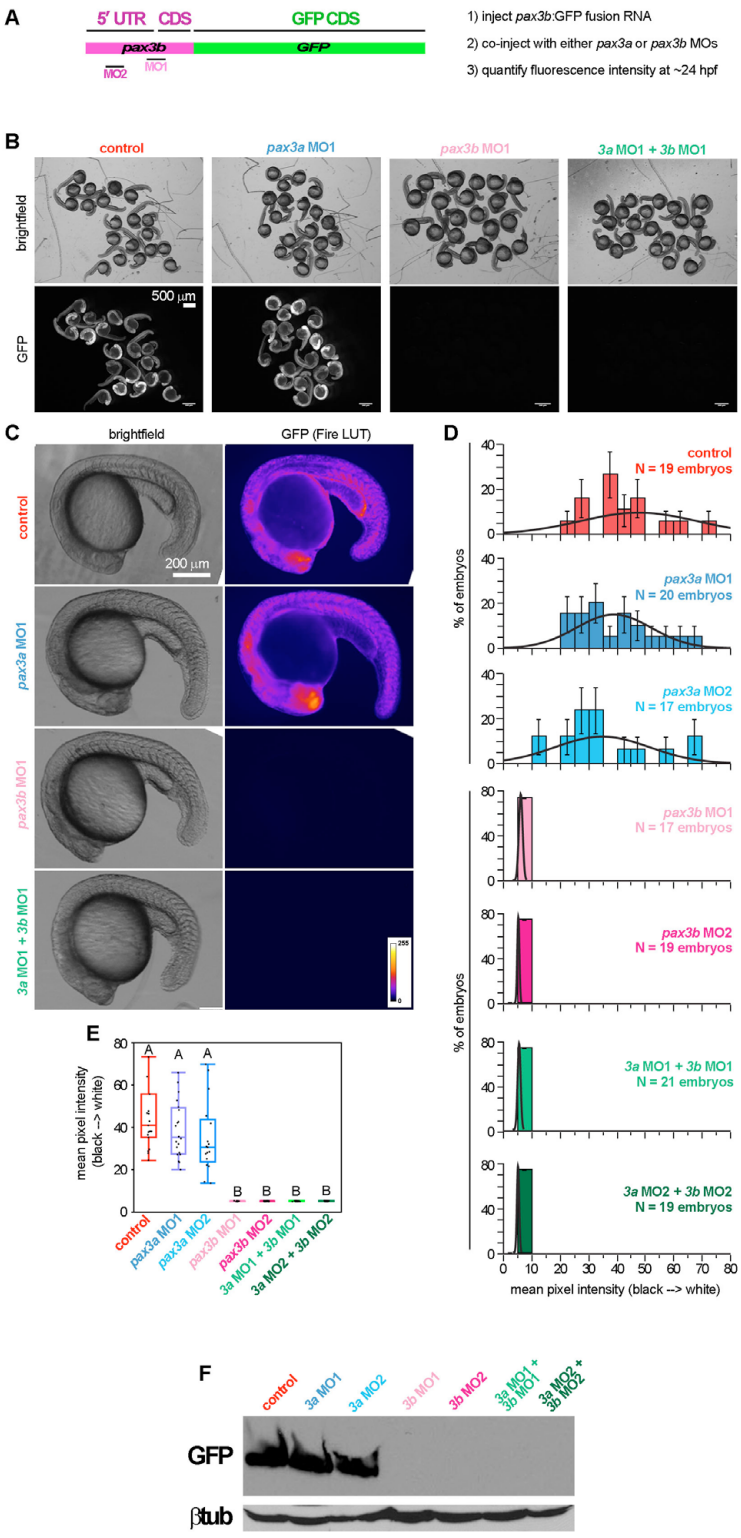

Fig. S9. *pax3b*, but not *pax3a*, MOs efficiently reduce translation of chimeric *5′UTRpax3b*:GFP RNA. (**A**) Primers (forward with *Xho*I site 5′-gcgctcgagtgatcgtggaatattacatg-3; reverse with *Bam*HI site 5′-gcgggatcc gagagtgatgggcgcatcat-3′) were used to amplify 62 bp of *pax3b* 5′UTR and 48 bp of *pax3b*-coding sequence. The resulting fragment was cloned in frame with EGFP in pEGFP-N1 (Invitrogen) to produce a *5′UTRpax3b:eGFP* fusion protein. *5′UTRpax3b:eGFP* was then subcloned into pSP64T, and RNA was transcribed using SP6 (Ambion). RNA (250 pg) was injected alone, or together with MO, into one-cell stage embryos. (**B**) At 24 hpf, embryos of control (*5′UTRpax3b:eGFP*) and *5′UTRpax3b:eGFP* plus *pax3a* MO1 or MO2 contained high levels of GFP fluorescence. Embryos with either *pax3b* MO had no detectable fluorescence, indicating complete inhibition of *5′UTRpax3b:eGFP* translation by *pax3b* MOs. (**C**) Images of single embryos were taken at identical magnifications and exposure. Background was normalized using the 'Subtract Background' feature of ImageJ (1.47n5). Pixel intensity of 8-bit greyscale images was visualized using the 'Fire' LUT. (**D**) Mean pixel intensity per embryo was normally distributed. (**E**) The mean pixel intensities were significantly reduced after addition of *pax3b* MO, as determined by ANOVA and Tukey's post hoc test. (**F**) Protein lysates were separated by 12% SDS-PAGE and probed using antibodies against GFP or β-tubulin (loading control).

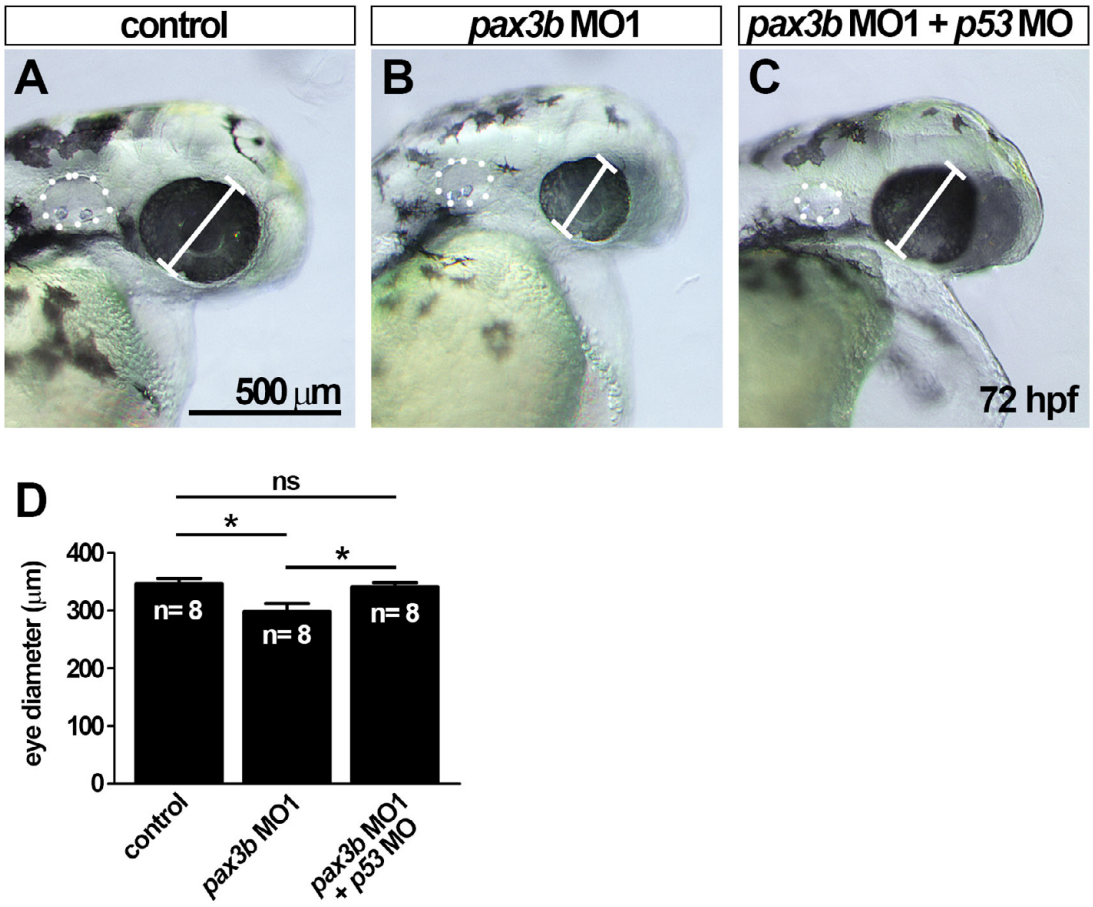

Fig. S10. *pax3b* MO1 induces a small eye phenotype that is rescued by co-injection of *p53* morpholino. (**A-C**) Bright-field images of eye in control (A), *pax3b* MO1-injected (B) and *pax3b* MO1- and *p53* MO-injected (C) larvae at 72 hpf. (**D**) Quantification of eye diameter reveals injection of *pax3b* MO1 leads to a smaller eye ($P<0.05$), that is rescued by co-injection of a *p53* MO (*$P<0.05$). One-way ANOVA followed by a Tukey's post hoc test.

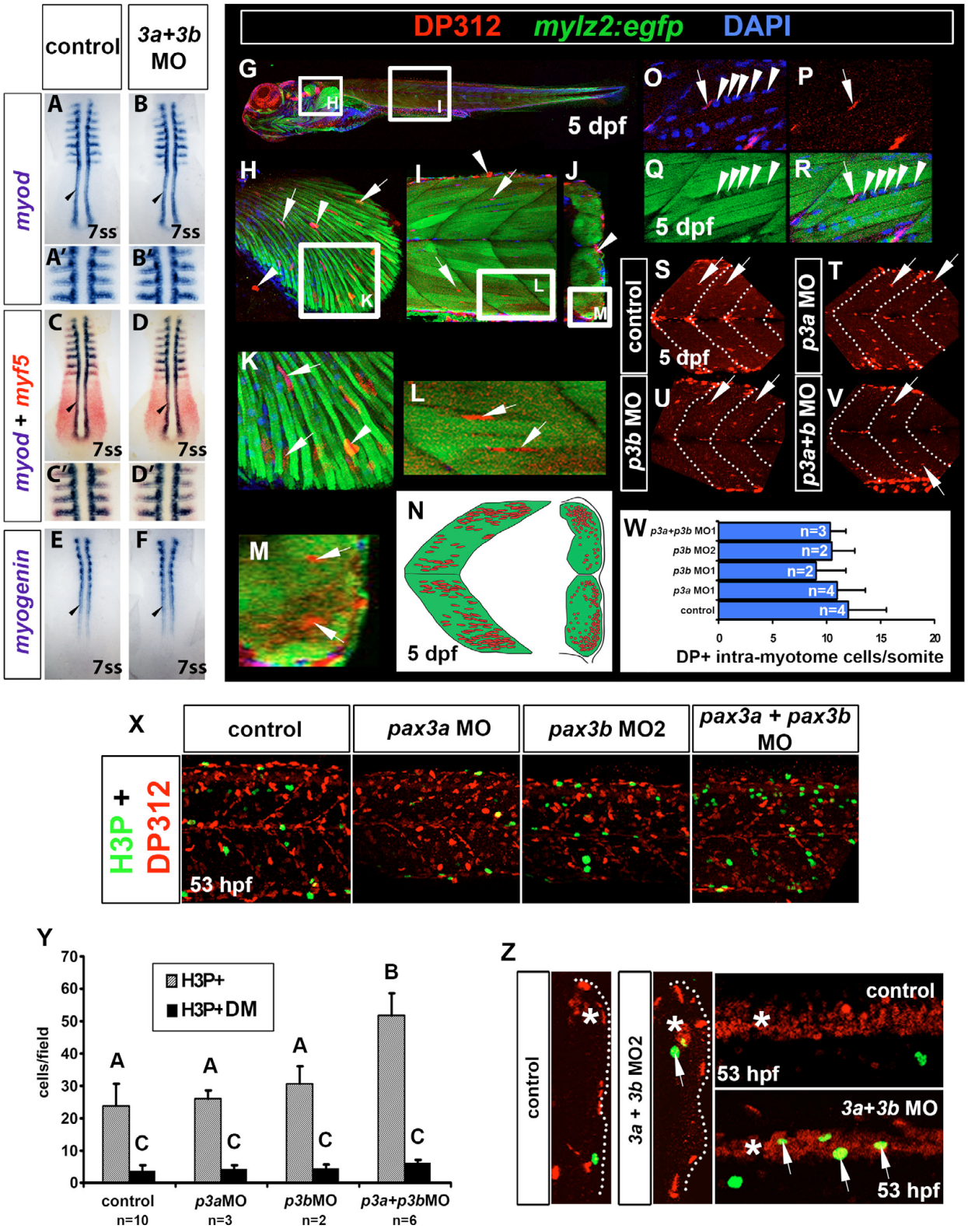

Fig. S11. Early myogenesis and Pax3/7^{+} intra-myotome cells occur normally in *pax3b* morphants. *In situ* hybridisation of *myod* (A-B′; blue, C-D′), *myf5* (red, C-D′) and *myogenin* (E,F). Immunodetection of DP312 (G-M,O-V; red, X,Z) and phospho-histone H3 (H3P) (green, X,Z) in wild-type (A-F,X,Z) and *Tg*(*mylz2:egfp*) backgrounds. (**A-F**) Expression of *myod*, *myf5* and *myog* at 7 ss are unaffected in *pax3a+pax3b* double morphants. (**G-M**) DP312^{+} intra-myotome cells (IMCs) localise to inter-fibre regions, reminiscent of Pax7^{+} myogenic cells (Seger et al., 2011). (**N**) IMC location. (**O-R**) IMCs are likely to be myogenic as they are observed closely juxtaposed to myogenic nuclei (Q,R, arrowheads) during myotube fusion (R). (**S-W**) Number of IMCs at 5 dpf is unchanged in *pax3a*, *pax3b* and *pax3a+pax3b* double morphants. (**X**,**Y**) Cell proliferation of dermomyotome cells (DM), as assessed by faint DP312/H3P^{+} nuclei (green, X) is unchanged after *pax3* manipulation (Y). However, total H3P^{+} nuclei are significantly increased in *pax3a+pax3b* double morphants (Y) (P<0.0001). (**Z**) Increase in H3P^{+} nuclei occurs in the neural tube. Asterisks indicate neural tube. Arrows indicate H3P^{+} nuclei within neural tube. One-way ANOVA and Tukey's post hoc test.

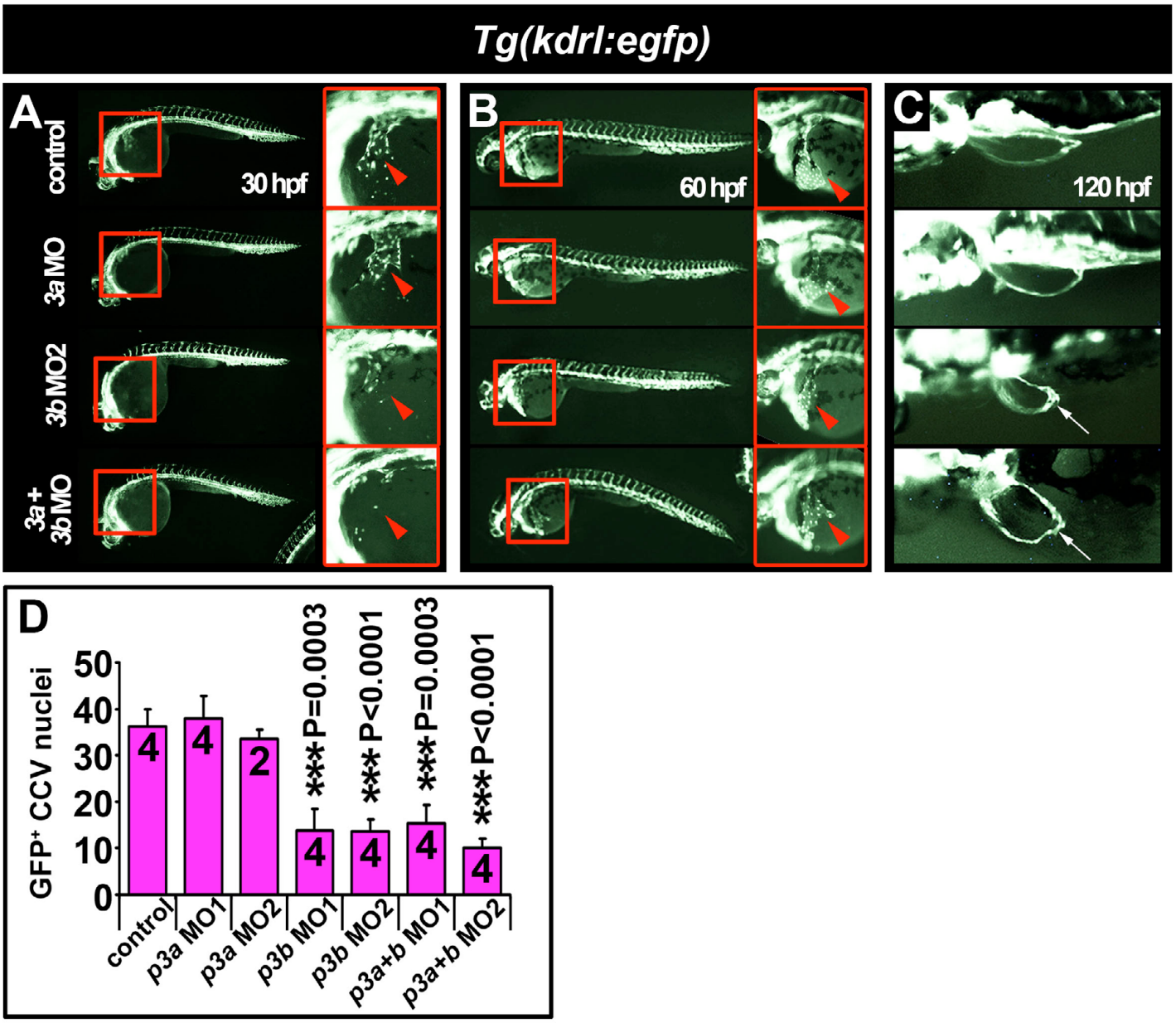

Fig. S12. Common cardinal vein development is delayed at 30 hpf in *pax3b* morphants. Fluorescent images of live embryos expressing eGFP under the *kdrl* (formerly known as *flk1* or *vegfr2*) promoter (A-C). Whole-mount lateral (A,B) or dorsal (C) views, anterior towards the left. (**A**) In 30 hpf embryos, general vasculogenesis was unimpaired after *pax3a/b* knockdown. However, the forming common cardinal vein (CCV) was reduced in *pax3b* single and double *pax3a/b* morphants (arrowheads). Boxed areas indicate regions magnified in the corresponding panels on the right. (**B**) In 60 hpf larvae, the general integrity of the vascular system was indistinguishable between control and *pax3a/b* morphants. Endothelial cells of the CCV had spread across the yolk (arrowheads). (**C**) Pectoral fin vasculature developed normally in *pax3a*, *pax3b* and *pax3a*+*pax3b* double morphants. The pectoral fin is malformed after *pax3b* manipulation (arrows). (**D**) Quantification of eGFP^{+} CCV nuclei at 30 hpf, mean±s.e.m. Sample number is indicated within each bar.

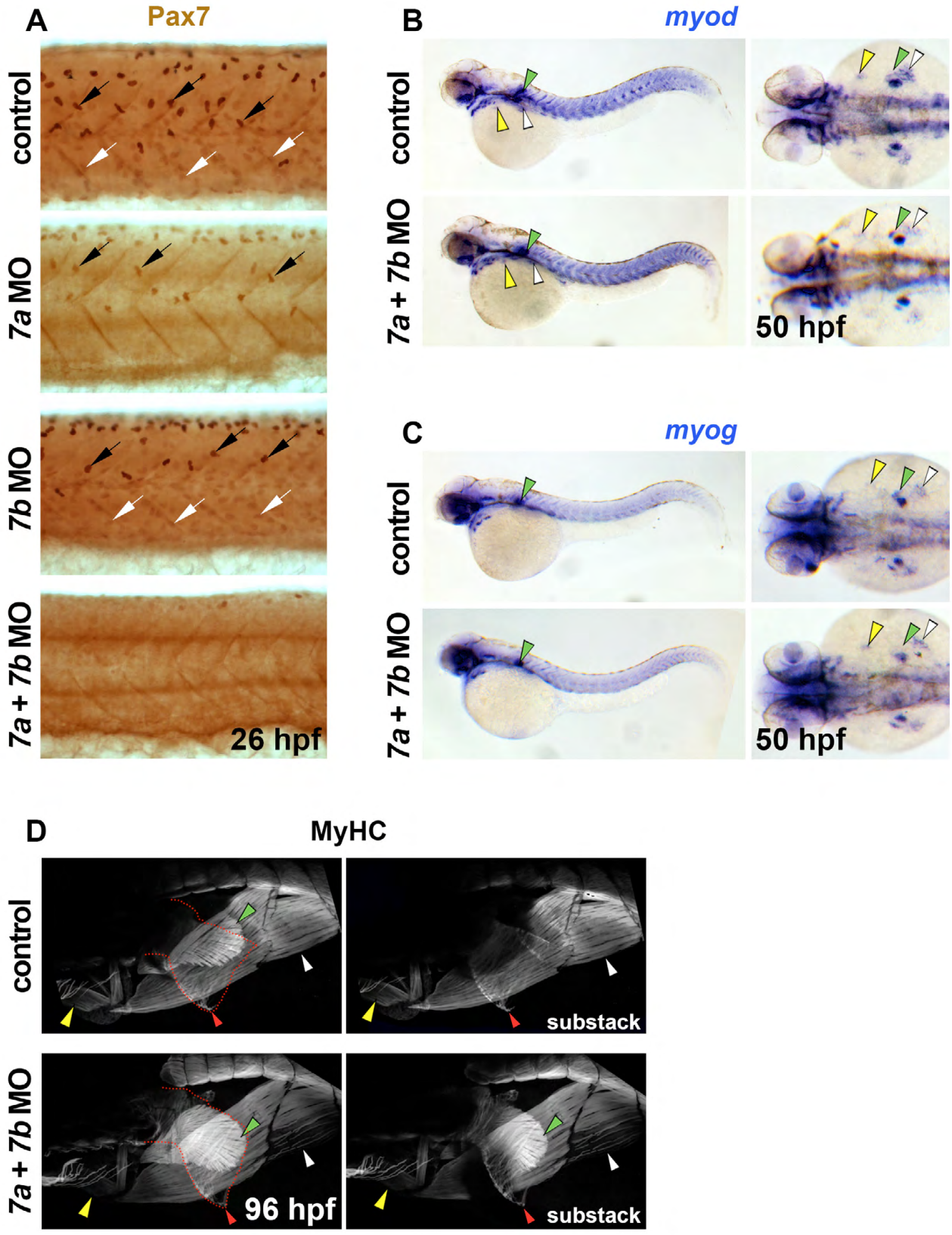

Fig. S13. Pax7 proteins are not required for MRF gene expression and subsequent hypaxial and oesophageal striated muscle formation. Immunodetection of Pax7 (A) and sarcomeric MyHC (D) or *in situ* mRNA hybridization for *myod* (B) and *myog* (C). Lateral view wholemounts have anterior towards the left and dorsal towards the top (A-C, left panels; D). Dorsal view wholemounts have anterior towards the left (B and C, right panels). (**A**) Nuclear Pax7 proteins accumulate weakly in dermomyotome cells (white arrows) and strongly in xanthophores (black arrows) overlying the somites at 26 hpf. Whereas *pax7a* MO diminishes dermomyotomal Pax7, both *pax7a* and *pax7b* MOs are required to remove all immunodetection. (**B**,**C**) Injection of dual *pax7a+pax7b* MOs has no discernible effect upon either *myod* (B) or *myog* (C) mRNA accumulation in anterior or posterior hypaxial muscle anlage or pectoral fin at 50 hpf (yellow, white and green arrowheads, respectively). (**D**) At 96 hpf, sarcomeric MyHC had accumulated in OSM (red markers) and extended caudally in both control and *pax7a+pax7b* morphant animals.

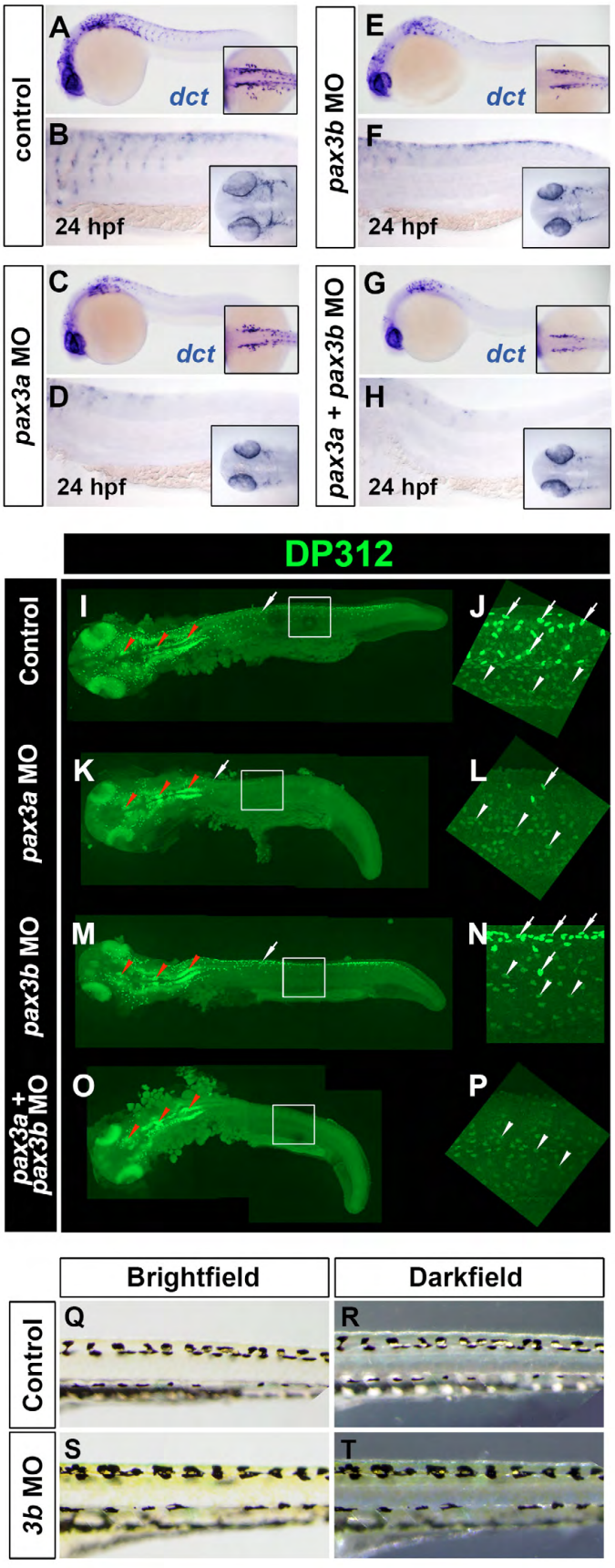

Fig. S14. Markers of neural crest are still expressed in *pax3b* morphants. *In situ* mRNA hybridisation of *dct* (A-H) and immunodetection of DP312 (I-O). Lateral view wholemounts are oriented anterior towards the left and dorsal towards the top (A-P); insets in A,C,E,G are wholemount dorsal views with anterior towards the left. Insets in B,D,F,H are dorsal views with anterior towards the left. (**A-H**) *dct* expression in melanoblasts is reduced in *pax3a* single and *pax3a+pax3b* double morphants (Minchin and Hughes, 2008), but *pax3b* morphants are similar to controls. (**I-P**) Intensely labelled DP312+ cells corresponding to xanthophores are still present in *pax3b* morphants (L). (**Q-T**) At 5 dpf, pigmentation is grossly normal in *pax3b* morphants.

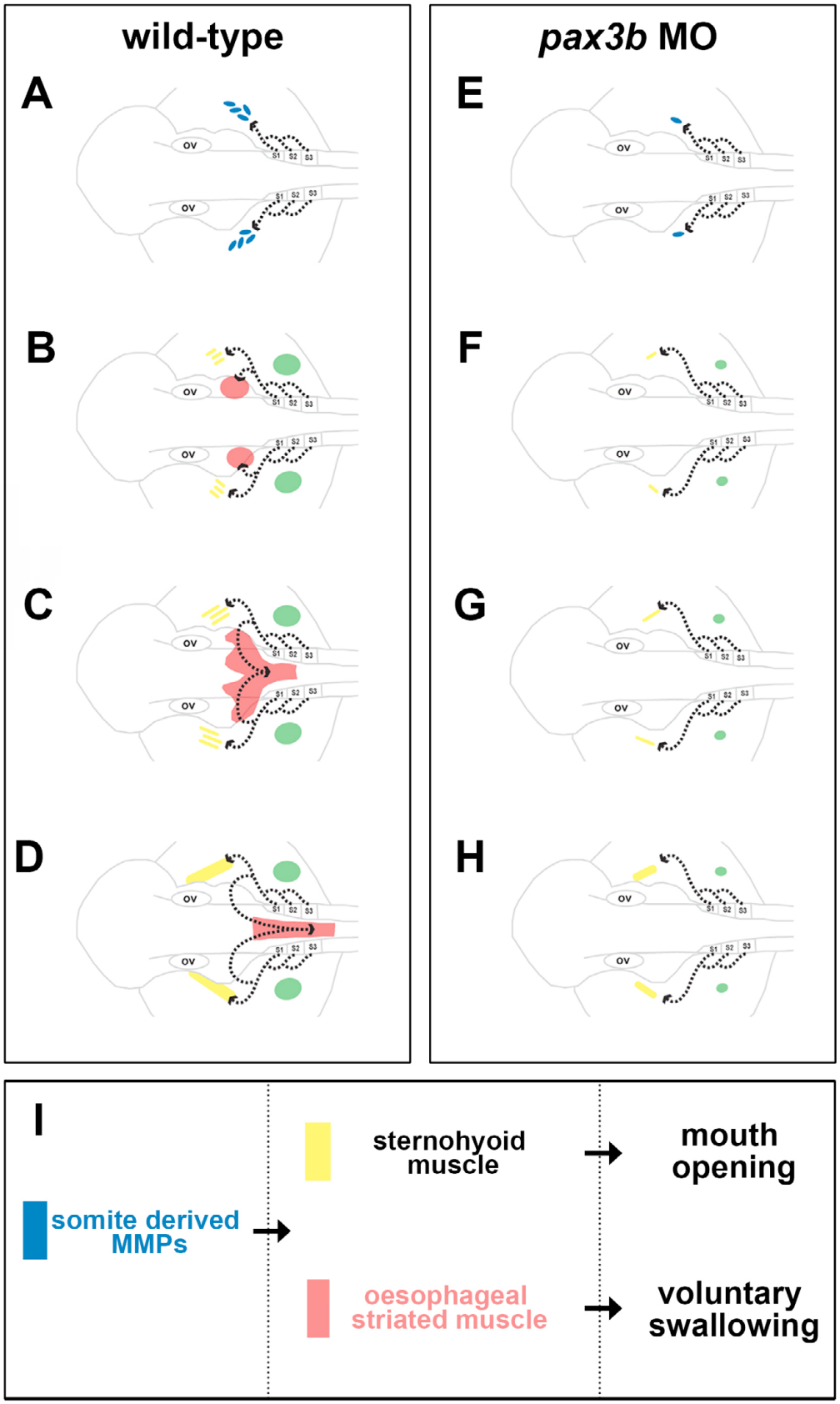

Fig. S15. Schematic of *pax3b*-dependent formation of OSM from migratory somite cells in zebrafish. (**A-I**) Model for migration of sternohyoideus and OSM precursors. MMPs migrate in a single stream from somites 1-3 (blue, A). Prior to 36 hpf, OSM precursors migrate medially to the oesophagus and begin expression of *myf5* (red, B). SHM precursors continue their rostral migration and SHM differentiation begins (yellow, B). Pectoral fin muscle begins to differentiate (green, B). It is unclear whether PFM precursors migrate along the same pathway as SHM and OSM. Bilateral myf5+ clusters begin to move medially and form an 'inverse fountain' (C). Differentiation of OSM is evident at the most posterior point (red, C). Migration of OSM is complete by 72 hpf, and differentiation is under way (red, D). Migration of MMPs (E), and differentiation of OSM, SHM and PFM are reduced in *pax3b* morphants (F-H).

Table S1.

Figure number and panel	Assay	Genotype/treatment	Sample number	% embryos affected
Fig4A	*myog* ISH, 72hpf	*myf5*+/hu2022 incross:	n=42	
		sibling and *myf5*hu2022		42/42 (100%)-normal *myog* in OSM
Fig4A	*mylz2* ISH, 120hpf	*myf5*+/hu2022 incross:	n=39	
		sibling and *myf5*hu2022		39/39 (100%)-normal *mylz2* in OSM
Fig4B	MF20 (MyHC);Myh11 IHC, 120hpf	sibling and *myf5*hu2022	n=35	35/35 (100%) normal for Myh11;MyHC in OSM
Fig4B	MF20 (MyHC);Myh11 IHC, 120hpf	sibling and *myf5*hu2022	48/59	48/48 (100%) normal for Myh11;MyHC in OSM
Fig4B	MF20 (MyHC);Myh11 IHC, 120hpf	*myod*fh261	7/59	7/7(100%) normal for Myh11;No MyHC in OSM
Fig4B	MF20 (MyHC);Myh11 IHC, 120hpf	*myf5*hu2022;*myod*fh261	4/59	4/4(100%) normal for Myh11No MyHC in OSM
Fig4 (data not shown)	MF20 (MyHC);Myh11 IHC, 120hpf	control	n=20	20/20 (100%) normal for Myh11;MyHC in OSM
Fig4 (data not shown)	MF20 (MyHC);Myh11 IHC, 120hpf	*myod* MO	n=37	33/37(89%)normal for Myh11;No MyHC in OSM
Fig4C	*myog* ISH, 72hpf	*myod*+/fh261 incross:	n=25	
		sibling	20/25	25/25 (100%)- normal *myog* in OSM
		*myod*fh261	5/25	5/5 (100%)-no *myog* in OSM
Fig4D	*myog* ISH, 72hpf	control	n=15	15/15 (100%)- normal *myog* in OSM
		myod MO	n=37	37/37 (100%)-reduced or absent *myog* in OSM
Fig5K-K''	*lbx2* ISH, 24hpf	control	n=38	38/38 (100%)-normal *lbx2* in migrating muscle precursors
Fig5M-M''	*lbx2* ISH, 24hpf	*pax3b* MO1	n=45	32/45 (71%)-reduced or absent *lbx2* in migrating muscle precursors
Fig5 (data not shown)	*lbx2* ISH, 24hpf	*pax3b* MO2	n=59	46/59 (78%)-reduced or absent *lbx2* in migrating muscle precursors
Fig5L-L''	*lbx2* ISH, 24hpf	*pax3a* MO1	n=40	38/40 (95%)-normal *lbx2* in migrating muscle precursors
Fig5 (data not shown)	*lbx2* ISH, 24hpf	*pax3a* MO2	n=56	50/56 (89%)-normal *lbx2* in migrating muscle precursors
Fig5N-N''	*lbx2* ISH, 24hpf	*pax3a* MO1 + *pax3b* MO1	n=66	55/66 (83%)-reduced or absent *lbx2* in migrating muscle precursors
Fig5 (data not shown)	*lbx2* ISH, 24hpf	*pax3b* MO2 + *pax3b* MO2	n=77	68/77 (88%)-reduced or absent *lbx2* in migrating muscle precursors
Fig6A	*myf5* ISH, 50hpf	control	n=23	23/23 (100%)-normal 'inverse *myf5* fountain'
Fig6B	*myf5* ISH, 50hpf	*pax3b* MO1	n=37	20/23 (87%)-absent 'inverse *myf5* fountain'
Fig6C	*myf5* ISH, 50hpf	*pax3a* MO1	n=25	25/25 (100%)-normal 'inverse *myf5* fountain'
Fig6D	*myf5* ISH, 50hpf	*pax3a* MO1 + *pax3b* MO1	n=26	18/23 (78%)-absent 'inverse *myf5* fountain'
Fig6E,E'	*myogenin* ISH, 53hpf	control	n=82	82/82 (100%)-normal *myog* in OSM
Fig6 (data not shown)	*myogenin* ISH, 53hpf	*pax3b* MO1	n=76	63/76 (82%)-*myog* reduced or absent in OSM
Fig6G,G'	*myogenin* ISH, 53hpf	*pax3b* MO2	n=93	85/93 (91%)-*myog* reduced or absent in OSM
Fig6F,F'	*myogenin* ISH, 53hpf	*pax3a* MO1	n=72	70/72 (97%)-normal *myog* in OSM
Fig6 (data not shown)	*myogenin* ISH, 53hpf	*pax3a* MO2	n=132	126/132 (95%)-normal *myog* in OSM

Fig6 (data not shown)	*myogenin* ISH, 53hpf	*pax3a* MO1 + *pax3b* MO1	n=80	60/80 (75%)-*myog* reduced or absent in OSM
Fig6H,H'	*myogenin* ISH, 53hpf	*pax3b* MO2 + *pax3b* MO2	n=96	81/96 (84%)-*myog* reduced or absent in OSM
Fig6E,E'	*myogenin* ISH, 53hpf	control	n=82	82/82 (100%)-normal *myog* in SHM/PFM and PHM
Fig6 (data not shown)	*myogenin* ISH, 53hpf	*pax3b* MO1	n=76	66/76 (86%)-reduced or absent *myog* in SHM/PFM and PHM
Fig6G,G'	*myogenin* ISH, 53hpf	*pax3b* MO2	n=93	71/93 (76%)-reduced or absent *myog* in SHM/PFM and PHM
Fig6F,F'	*myogenin* ISH, 53hpf	*pax3a* MO1	n=72	68/72 (94%)-normal *myog* in SHM/PFM and PHM
Fig6 (data not shown)	*myogenin* ISH, 53hpf	*pax3a* MO2	n=132	120/132 (91%)-normal *myog* in SHM/PFM and PHM
Fig6 (data not shown)	*myogenin* ISH, 53hpf	*pax3a* MO1 + *pax3b* MO1	n=80	67/80 (84%)-reduced or absent *myog* in SHM/PFM and PHM
Fig6H,H'	*myogenin* ISH, 53hpf	*pax3b* MO2 + *pax3b* MO2	n=96	75/96 (78%)-reduced or absent *myog* in SHM/PFM and PHM
Fig6I	MF20 (MyHC) IHC, 96hpf	control	n=35	35/35 (100%)-normal MyHC in OSM
Fig6K	MF20 (MyHC) IHC, 96hpf	*pax3b* MO1	n=52	40/52 (77%)-reduced MyHC in OSM
Fig6 (data not shown)	MF20 (MyHC) IHC, 96hpf	*pax3b* MO2	n=28	20/28 (71%)-reduced MyHC in OSM
Fig6J	MF20 (MyHC) IHC, 96hpf	*pax3a* MO1	n=45	45/45 (100%)-normal MyHC in OSM
Fig6 (data not shown)	MF20 (MyHC) IHC, 96hpf	*pax3a* MO2	n=58	58/58 (100%)-normal MyHC in OSM
Fig6L	MF20 (MyHC) IHC, 96hpf	*pax3a* MO1 + *pax3b* MO1	n=34	30/34 (88%)-reduced MyHC in OSM
Fig6 (data not shown)	MF20 (MyHC) IHC, 96hpf	*pax3b* MO2 + *pax3b* MO2	n=21	17/21 (81%)-reduced MyHC in OSM
Fig6M	MF20 (MyHC) IHC, 96hpf	control	n=35	35/35 (100%)-normal MyHC in TV
Fig6O	MF20 (MyHC) IHC, 96hpf	*pax3b* MO1	n=52	52/52 (100%)-normal MyHC in TV
Fig6 (data not shown)	MF20 (MyHC) IHC, 96hpf	*pax3b* MO2	n=28	28/28 (100%)-normal MyHC in TV
Fig6N	MF20 (MyHC) IHC, 96hpf	*pax3a* MO1	n=45	45/45 (100%)-normal MyHC in TV
Fig6 (data not shown)	MF20 (MyHC) IHC, 96hpf	*pax3a* MO2	n=58	58/58 (100%)-normal MyHC in TV
Fig6P	MF20 (MyHC) IHC, 96hpf	*pax3a* MO1 + *pax3b* MO1	n=34	34/34 (100%)-normal MyHC in TV
Fig6 (data not shown)	MF20 (MyHC) IHC, 96hpf	*pax3b* MO2 + *pax3b* MO2	n=21	21/21 (100%)-normal MyHC in TV
Fig6S	Myh11 IHC, 96hpf	control	n=22	22/22 (100%)-normal smooth Myosin in GIT
Fig6 (data not shown)	Myh11 IHC, 96hpf	*pax3b* MO2	n=20	20/20 (100%)-normal smooth Myosin in GIT
Fig6T	Myh11 IHC, 96hpf	*pax3a* MO1	n=39	39/39 (100%)-normal smooth Myosin in GIT
Fig6 (data not shown)	Myh11 IHC, 96hpf	*pax3a* MO2	n=21	21/21 (100%)-normal smooth Myosin in GIT
Fig6V	Myh11 IHC, 96hpf	*pax3a* MO1 + *pax3b* MO1	n=25	25/25 (100%)-normal smooth Myosin in GIT
Fig6 (data not shown)	Myh11 IHC, 96hpf	*pax3b* MO2 + *pax3b* MO2	n=26	26/26 (100%)-normal smooth Myosin in GIT
Fig7A	Tg(*actc1b*:*egfp*), 120hpf	control	n=179	179/179 (100%)-normal Gfp in SHM/PFM and PHM
Fig7A	Tg(*actc1b*:*egfp*), 120hpf	*pax3b* MO1	n=126	101/126 (80%)-both mild and severely reduced Gfp in SHM/PFM and PHM
Fig7 (data not shown)	Tg(*actc1b*:*egfp*), 120hpf	*pax3b* MO2	n=73	55/73 (75%)-both mild and severely reduced Gfp in SHM/PFM and PHM
Fig7A	Tg(*actc1b*:*egfp*), 120hpf	*pax3a* MO1	n=55	54/55 (98%)-normal Gfp in SHM/PFM and PHM
Fig7 (data not shown)	Tg(*actc1b*:*egfp*), 120hpf	*pax3a* MO2	n=34	34/34 (100%)-normal Gfp in SHM/PFM and PHM
Fig7A	Tg(*actc1b*:*egfp*), 120hpf	*pax3a* MO1 + *pax3b* MO1	n=79	59/79 (73%)-both mild and severely reduced Gfp in SHM/PFM and PHM

Fig7H	microspheres, 120hpf	*control*	n=38	38/38 (100%)-normal quantity of internalised microspheres
Fig7H	microspheres, 120hpf	*pax3b* MO1	n=53	48/53 (91%)-reduced internalised microspheres
Fig7H	microspheres, 120hpf	*pax3a* MO1	n=27	27/27 (100%)-normal quantity of internalised microspheres
Fig7H	microspheres, 120hpf	*pax3a* MO1 + *pax3b* MO1	n=44	42/44 (95%)-reduced internalised microspheres
Suppl. Fig8E,E'	DP312 IHC, 7ss	control	n=25	25/25 (100%)-normal DP312 reactivity
Suppl. Fig8F	DP312 IHC, 7ss	*pax3a* MO1	n=35	33/35 (94%)-absent DP312 reactivity in *pax3a* regions
Suppl. Fig8 (data not shown)	DP312 IHC, 7ss	*pax3a* MO2	n=22	19/22 (86%)-absent DP312 reactivity in *pax3a* regions
Suppl. Fig8G	DP312 IHC, 7ss	*pax3b* MO1	n=116	116/116 (100%)-normal DP312 reactivity
Suppl. Fig8 (data not shown)	DP312 IHC, 7ss	*pax3b* MO2	n=136	136/136 (100%)-normal DP312 reactivity
Suppl. Fig8H	DP312 IHC, 7ss	*pax3a* MO1 + *pax3b* MO1	n=87	78/87 (89%)-absent DP312 reactivity in *pax3a* and *pax3b* regions
Suppl. Fig8 (data not shown)	DP312 IHC, 7ss	*pax3b* MO2 + *pax3b* MO2	n=102	82/102 (78%)-absent DP312 reactivity in *pax3a* and *pax3b* regions
Suppl. Fig8I	*transgelin* ISH, 96hpf	control	n=19	19/19 (100%)-normal *transgelin* in GIT
Suppl. Fig8I	*transgelin* ISH, 96hpf	*pax3b* MO1	n=30	30/30 (100%)-normal *transgelin* in GIT
Suppl. Fig8 (data not shown)	*transgelin* ISH, 96hpf	*pax3b* MO2	n=27	27/27 (100%)-normal *transgelin* in GIT
Suppl. Fig8I	*transgelin* ISH, 96hpf	*pax3a* MO1	n=24	24/24 (100%)-normal *transgelin* in GIT
Suppl. Fig8 (data not shown)	*transgelin* ISH, 96hpf	*pax3a* MO2	n=17	17/17 (100%)-normal *transgelin* in GIT
Suppl. Fig8I	*transgelin* ISH, 96hpf	*pax3a* MO1 + *pax3b* MO1	n=20	20/20 (100%)-normal *transgelin* in GIT
Suppl. Fig8 (data not shown)	*transgelin* ISH, 96hpf	*pax3b* MO2 + *pax3b* MO2	n=29	29/29 (100%)-normal *transgelin* in GIT
Suppl. Fig8J	*myogenin* ISH, 53hpf	control	n=82	82/82 (100%)-normal *myog* in OSM
Suppl. Fig8 (data not shown)	*myogenin* ISH, 53hpf	*pax3b* MO1	n=76	63/76 (82%)-*myog* reduced or absent in OSM
Suppl. Fig8J	*myogenin* ISH, 53hpf	*pax3b* MO2	n=93	85/93 (91%)-*myog* reduced or absent in OSM
Suppl. Fig8J	*myogenin* ISH, 53hpf	*pax3a* MO1	n=72	70/72 (97%)-normal *myog* in OSM
Suppl. Fig8 (data not shown)	*myogenin* ISH, 53hpf	*pax3a* MO2	n=132	126/132 (95%)-normal *myog* in OSM
Suppl. Fig8 (data not shown)	*myogenin* ISH, 53hpf	*pax3a* MO1 + *pax3b* MO1	n=80	60/80 (75%)-*myog* reduced or absent in OSM
Suppl. Fig8J	*myogenin* ISH, 53hpf	*pax3b* MO2 + *pax3b* MO2	n=96	81/96 (84%)-*myog* reduced or absent in OSM
Suppl. Fig10A	brightfield, 72hpf	control	n=15	15/15 (100%)-normal eye size
Suppl. Fig10B	brightfield, 72hpf	*pax3b* MO1	n=24	20/24 (83%)-small eye size
Suppl. Fig10C	brightfield, 72hpf	*pax3b* MO1 + p53 MO	n=31	20/31 (65%)-normal eye size
Suppl. Fig11A	*myod* ISH, 7ss	control	n=15	
Suppl. Fig11B	*myod* ISH, 7ss	*pax3a* MO1 + *pax3b* MO1	n=23	
Suppl. Fig11C	*myod* + myf5 ISH, 7ss	control	n=24	
Suppl. Fig11D	*myod* + *myf5* ISH, 7ss	*pax3a* MO1 + *pax3b* MO1	n=25	
Suppl. Fig11C	*myog* ISH, 7ss	control	n=26	

Suppl. Fig11D	*myog* ISH, 7ss	*pax3a* MO1 + *pax3b* MO1	n=19	
Suppl. Fig11S	DP312 IHC, 5dpf	control	n=22	
Suppl. Fig11T	DP312 IHC, 5dpf	*pax3a* MO1	n=27	
Suppl. Fig11U	DP312 IHC, 5dpf	*pax3b* MO2	n=20	
Suppl. Fig11V	DP312 IHC, 5dpf	*pax3a* MO1 + *pax3b* MO1	n=21	
Suppl. Fig11X	DP312 + H3P IHC, 53hpf	control	n=25	
Suppl. Fig11X	DP312 + H3P IHC, 53hpf	*pax3b* MO2	n=31	
Suppl. Fig11X	DP312 + H3P IHC, 53hpf	*pax3a* MO1 + *pax3b* MO1	n=38	
Suppl. Fig12A	Tg(*kdrl*:*egfp*), 30hpf	control	n=27	27/27 (100%)-normal Gfp+ CCV endothelial cells
Suppl. Fig12 (data not shown)	Tg(*kdrl*:*egfp*), 30hpf	*pax3a* MO1	n=23	23/23 (100%)-normal Gfp+ CCV endothelial cells
Suppl. Fig12 (data not shown)	Tg(*kdrl*:*egfp*), 30hpf	*pax3b* MO1	n=29	22/29 (76%)-reduced or absent Gfp+ CCV endothelial cells
Suppl. Fig12A	Tg(*kdrl*:*egfp*), 30hpf	*pax3b* MO2	n=35	31/35 (89%)-reduced or absent Gfp+ CCV endothelial cells
Suppl. Fig12 (data not shown)	Tg(*kdrl*:*egfp*), 30hpf	*pax3a* MO1 + *pax3b* MO1	n=29	25/29 (86%)-reduced or absent Gfp+ CCV endothelial cells
Suppl. Fig12A	Tg(*kdrl*:*egfp*), 30hpf	*pax3b* MO2 + *pax3b* MO2	n=26	25/26 (96%)-reduced or absent Gfp+ CCV endothelial cells
Suppl. Fig12B	Tg(*kdrl*:*egfp*), 60hpf	control	n=27	27/27 (100%)-normal Gfp+ CCV endothelial cells
Suppl. Fig12 (data not shown)	Tg(*kdrl*:*egfp*), 60hpf	*pax3a* MO1	n=23	23/23 (100%)-normal Gfp+ CCV endothelial cells
Suppl. Fig12B	Tg(*kdrl*:*egfp*), 60hpf	*pax3a* MO2	n=34	34/34 (100%)-normal Gfp+ CCV endothelial cells
Suppl. Fig12 (data not shown)	Tg(*kdrl*:*egfp*), 60hpf	*pax3b* MO1	n=29	25/29 (86%)-normal Gfp+ CCV endothelial cells
Suppl. Fig12B	Tg(*kdrl*:*egfp*), 60hpf	*pax3b* MO2	n=35	33/35 (94%)-normal Gfp+ CCV endothelial cells
Suppl. Fig12 (data not shown)	Tg(*kdrl*:*egfp*), 60hpf	*pax3a* MO1 + *pax3b* MO1	n=29	28/29 (97%)-normal Gfp+ CCV endothelial cells
Suppl. Fig12B	Tg(*kdrl*:*egfp*), 60hpf	*pax3b* MO2 + *pax3b* MO2	n=26	23/26 (88%)-normal Gfp+ CCV endothelial cells
Suppl. Fig12C	Tg(*kdrl*:*egfp*), 120hpf	control	n=27	27/27 (100%)-normal Gfp+ PFV endothelial cells
Suppl. Fig12 (data not shown)	Tg(*kdrl*:*egfp*), 120hpf	*pax3a* MO1	n=23	23/23 (100%)-normal Gfp+ PFV endothelial cells
Suppl. Fig12C	Tg(*kdrl*:*egfp*), 120hpf	*pax3a* MO2	n=34	34/34 (100%)-normal Gfp+ PFV endothelial cells
Suppl. Fig12 (data not shown)	Tg(*kdrl*:*egfp*), 120hpf	*pax3b* MO1	n=29	29/29 (100%)-normal Gfp+ PFV endothelial cells
Suppl. Fig12C	Tg(*kdrl*:*egfp*), 120hpf	*pax3b* MO2	n=35	35/35 (100%)-normal Gfp+ PFV endothelial cells
Suppl. Fig12 (data not shown)	Tg(*kdrl*:*egfp*), 120hpf	*pax3a* MO1 + *pax3b* MO1	n=29	29/29 (100%)-normal Gfp+ PFV endothelial cells
Suppl. Fig12C	Tg(*kdrl*:*egfp*), 120hpf	*pax3b* MO2 + *pax3b* MO2	n=26	26/26 (100%)-normal Gfp+ PFV endothelial cells
Suppl. Fig13A	Pax7 IHC, 26hpf	control	n=12	12/12 (100%)-normal Pax7 protein in xanthophores (intense stain) and dermomyotome (weak stain)
Suppl. Fig13A	Pax7 IHC, 26hpf	pax7a MO	n=15	15/15 (100%)-weak Pax7 protein in dermomyotome (weak stain) and reduced xanthophores nuclei (intense stain)
Suppl. Fig13A	Pax7 IHC, 26hpf	pax7b MO	n=21	21/21 (100%)-normal Pax7 protein in xanthophores (intense stain) and

Suppl. Fig13A	Pax7 IHC, 26hpf	pax7a+7b MO	n=2	dermomyotome (weak stain) 2/2 (100%)-ablated Pax7 protein in dermomyotome (weak stain) and xanthophores (intense stain)
Suppl. Fig13B	myod ISH, 50hpf	control	n=29	29/29 (100%)-myod expression in hypaxial-derived muscles
Suppl. Fig13B	myod ISH, 50hpf	pax7a+7b MO	n=31	31/31 (100%)-myod expression in hypaxial-derived muscles
Suppl. Fig13C	myog ISH, 50hpf	control	n=15	15/15 (100%)-myod expression in hypaxial-derived muscles
Suppl. Fig13C	myog ISH, 50hpf	pax7a+7b MO	n=25	25/25 (100%)-myod expression in hypaxial-derived muscles
Suppl. Fig13D	MyHC IHC, 96hpf	control	n=10	10/10 (100%)-MyHC in OSM
Suppl. Fig13D	MyHC IHC, 96hpf	pax7a+7b MO	n=9	9/9 (100%)-MyHC in OSM
Suppl. Fig14A,B	*dct* ISH, 24hpf	control	n=26	26/26 (100%)-normal dct expression
Suppl. Fig14C,D	*dct* ISH, 24hpf	*pax3a* MO1	n=25	20/25 (80%)-reduced dct expression
Suppl. Fig14E,F	*dct* ISH, 24hpf	*pax3b* MO2	n=32	29/32 (91%)-reduced dct expression
Suppl. Fig14G,H	*dct* ISH, 24hpf	*pax3a* MO1 + *pax3b* MO1	n=29	25/29 (86%)-reduced dct expression
Suppl. Fig14I,J	DP312 IHC, 24hpf	control	n=20	20/20 (100%)-normal DP+ xanthophores
Suppl. Fig14K,L	DP312 IHC, 24hpf	*pax3a* MO1	n=19	15/19 (79%)-reduced DP+ xanthophores
Suppl. Fig14M,N	DP312 IHC, 24hpf	*pax3b* MO2	n=22	22/22 (100%)-normal DP+ xanthophores
Suppl. Fig14O,P	DP312 IHC, 24hpf	*pax3a* MO1 + *pax3b* MO1	n=21	21/21 (100%)-normal DP+ xanthophores

CCV= common cardinal vein
GIT= gastrointestinal tract
OSM= oesophageal striated muscle
PFM= pectoral fin muscle
PFV= pectoral fin vasculature
PHM= posterior hypaxial muscle
SHM= sternohyoideus muscle
TV= tranvervus ventralis

Table S2. Morpholino sequences used for zebrafish experiments

Gene	Sequence (5′→3′)	Amount of MO injected (ng)	Reference
pax3a MO1	CTAATGCGGTCATATCTCCTCTGCA	4	Minchin and Hughes (2008)
pax3a MO2	AAAGGATGCACGAAGCACTTGATAG	2	Minchin and Hughes (2008)
pax3b MO1	CCTGGGAAAGCGGTCATTGCTCCG	2	
pax3b MO2	AGCGTTGACCAAAATCTTAGGACTT	4	
myod	ATATCCGACAACTCCATCTTTTTTG	4	Hinits et al. (2009)
p53	GCGCCATTGCTTTGCAAGAATTG	3	Robu et al. (2007)

Table S3. Probes for *in situ* mRNA hybridisation in zebrafish

Gene	Reference
pax3a	Seo et al. (1998)
pax3b	Minchin and Hughes (2008)
pax7a	Seo et al. (1998)
pax7b	Minchin and Hughes (2008)
myf5	Groves et al. (2005)
myod	Weinberg et al. (1996)
myog	Weinberg et al. (1996)
mylz2	Xu et al. (2000)
lbx2	Neyt et al. (2000)
dlx2a	Akimenko et al. (1994)
dct	Kelsh et al. (2000)

Table S4. Primers for qRT-PCR and the role of the protein encoded

Gene	Metabolic process	Reference
phospholipase A2 group 1b (*pla2g1b*)	Lipid metabolism	(Hama et al., 2009)
adiponectin receptor 1a (*adipor1a*)	Glucose/lipid metabolism	(Nishio et al., 2008)
amylase (*amyl*)	Glucose metabolism	(Imrie and Sadler, 2010)
fatty acid binding protein 10 (*fabp10*)	Lipid metabolism	(Imrie and Sadler, 2010)
peroxisome proliferator-activated receptor ɣ (*pparg*)	Glucose/lipid metabolism	(Imrie and Sadler, 2010)

Table S5. Quantification of fate mapping in mouse

Age	Genotype	Number of animals sectioned	Result
E15.5	*Pax3$^{Cre/+}$; Z/AP*	3	Only the most rostral section of the oesophagus has sarcomeric myosin at this stage. Several sections were found in each animal to contain between 1 and 10 AP+/sarcomeric MyHC+ cells.
E15.5	*Pax3$^{Cre/+}$; R26R*	4	Only the most rostral section of the oesophagus has sarcomeric myosin at this stage. Several sections where seen within each animal to contain between 1 and 10 EYFP+/sarcomeric MyHC+ cells (see Fig. 1B).
E17.5	*Pax3$^{Cre/+}$; R26R*	2	A larger area of the oesophagus contains sarcomeric myosin, many MyHC+ cells are weakly EYFP+.
P0	*Pax3$^{Cre/+}$; Z/AP*	1	A much larger area of the rostral oesophagus has sarcomeric myosin, with many fibres being AP^{+}. Fig.1C is a fair representation of most of this area.

Table S6. Quantification of *Pax7*^{CE} contribution to muscle fibres in outer and inner OSM layers

	Tam E9.5	**Tam E10.5**	**Tam E11.5**	**Tam E12.5**
Outer layer	14	20	128	210
	10	32	149	245
	7	23	152	198
Mean	10.3	25	143	217.7
Standard deviation	3.5	6.2	13.1	24.4
Inner layer	0	0	10	16
	0	1	6	13
	0	0	12	21
Mean	0	0.3	9.3	16.7
Standard deviation	0	0.6	3.1	4.0

Number of X-gal-labelled cells per section are shown.